

DOE/ER/40762-323

UM-PP#05-008

Deuteron Compton Scattering in Effective Field Theory And Spin-Independent Nucleon Polarizabilities

Jiunn-Wei Chen,^{1,*} Xiangdong Ji,^{2,†} and Yingchuan Li^{2,‡}

¹*Department of Physics and National Center for Theoretical Sciences at Taipei,
National Taiwan University, Taipei, Taiwan 10617*

²*Department of Physics, University of Maryland, College Park, Maryland 20742*

(Dated: August 11, 2018)

Abstract

Deuteron Compton scattering is calculated to $\mathcal{O}(Q^2)$ in pionless effective field theory using a dibaryon approach. The vector amplitude, which was not included in the previous pionless calculations, contributes to the cross section at $\mathcal{O}(Q^2)$ and influences significantly the extracted values of nucleon electric polarizability at incident photon energy 49 MeV. We recommend future high precision deuteron compton scattering experiments being performed at 25-35 MeV photon energy where the nucleon polarizability effects are appreciable and the pionless effective field theory is most reliable. For example, a measurement at 30 MeV with a 3% error will constrain the isoscalar nucleon electric polarizability α_0 with a $\sim 30\%$ error.

*Electronic address: jwc@phys.ntu.edu.tw

†Electronic address: xji@physics.umd.edu

‡Electronic address: yli@physics.umd.edu

I. INTRODUCTION

Nucleon polarizabilities are fundamental properties of nucleons. They characterize how easily the nucleons deform under external electromagnetic fields. For proton polarizabilities, tight constraints have been obtained by Compton scattering [1, 2, 3] and photoproduction sum rule [2, 3]. For neutron polarizabilities, the extraction is more complicated and less satisfactory. Scattering neutrons off the Coulomb field of a heavy nucleus could in principle determine the neutron electric polarizability [4, 5, 6, 7]. However, the error is still quite large. By far the best methods known to measure the neutron polarizabilities involve photon scattering on deuteron targets. This introduces theoretical complications such as final-state interactions and two-body currents.

Recently quasi-free Compton scattering ($\gamma d \rightarrow \gamma np$) at 200 to 400 MeV photon energy was carried out at Mainz [8]. Using the model developed in Ref. [9], tight constraints were reported on the neutron electric and magnetic polarizabilities: $\alpha_n = 12.5 \pm 1.8(\text{stat})^{+1.1}_{-0.6}(\text{syst}) \pm 1.1(\text{model})$ and $\beta_n = 2.7 \pm 1.8(\text{stat})^{+0.6}_{-1.1}(\text{syst}) \pm 1.1(\text{model})$ in units of 10^{-4} fm^3 (which will be used throughout this paper) [8]. The other approach, deuteron Compton scattering ($\gamma d \rightarrow \gamma d$), was carried out at Illinois [10], SAL (Saskatoon) [11] and Lund [12] with photon energy from 49 to 95 MeV. Several theoretical calculations are performed using potential models [13, 14, 15, 16]. The latest calculation using the Lund data at 55 and 66 MeV gives the iso-scalar combinations of nucleon polarizabilities $\alpha_0 + \beta_0 = 17.4 \pm 3.7$ and $\alpha_0 - \beta_0 = 6.4 \pm 2.4$ which, when combined with the proton values, imply $\alpha_n = 8.8 \pm 2.4(\text{total}) \pm 3.0(\text{model})$ and $\beta_n = 6.5 \pm 2.4(\text{total}) \pm 3.0(\text{model})$.

An alternative method to analyze deuteron Compton scattering is nuclear effective field theory (EFT) [17, 18] (see Ref. [19] for a recent review). The goal of the nuclear EFT program is to establish model independent, systematic and controlled expansions for few-body and eventually nuclear matter problems. For systems with characteristic momenta below the pion mass, theories with pions integrated out are highly successful and applied to many observables [18, 21, 22, 23, 24, 25]. For systems with characteristic momenta above the pion mass, power counting is more complicated [26]. But for practical purposes, the power counting developed by Weinberg [17] could still be quite accurate despite its renormalization problem in the 1S_0 channel. EFT calculations of deuteron Compton scattering were carried out in Refs. [3, 27, 28, 29]. The latest extraction of nucleon polarizabilities using Weinberg's theory but with phenomenological wave functions yields $\alpha_0 = 8.9 \pm 1.5^{+4.7}_{-0.9}$ and $\beta_0 = 2.2 \pm 1.5^{+1.2}_{-0.9}$ [3]. In comparison, using a theory with pion integrated out, Ref. [29] extracts $\alpha_0 = 8.4 \pm 3.4$ and $\beta_0 = 8.9 \pm 4.3$ from the 49 MeV data. Other calculations [27, 28] showed that data below 70 MeV give results consistent with the values predicted by leading-order chiral perturbation theory $\alpha_0 = 10\beta_0 = 12$ [20].

In the future, the High-Intensity Gamma Source (HIGS) at Duke University will be able to measure deuteron Compton scattering with high precision. Thus it is timely to ask what the best strategy is to improve the determination of nucleon polarizabilities. In this work, we focus on the low energy experiments—because the relevant theory is most well understood—and explore the sensitivity of α_0 and β_0 in future experiments. We follow the power counting in [28], and present the complete unpolarized deuteron Compton scattering cross section to $\mathcal{O}(Q^2)$ in the pionless dibaryon EFT [21, 24, 28]. A vector amplitude, which was not included in the previous pionless calculations was found to contribute at the same order as the nucleon polarizability contribution. The impact of the new contribution to the extraction of nucleon polarizabilities α_0 and β_0 is studied.

II. KINEMATICS

The number of independent structures in Compton scattering amplitudes can be conveniently analyzed in the helicity basis. In this basis, amplitudes are characterized by $\langle h'_1, h'_2 | h_1, h_2 \rangle$, where $h_i(h'_i)$ is the helicity for particle i in the initial(final) state. Under parity transformation (P), a helicity amplitude transforms as

$$P : \langle h'_1, h'_2 | h_1, h_2 \rangle \rightarrow \langle -h'_1, -h'_2 | -h_1, -h_2 \rangle . \quad (1)$$

While under time reversal transformation (T),

$$T : \langle h'_1, h'_2 | h_1, h_2 \rangle \rightarrow \langle h_1, h_2 | h'_1, h'_2 \rangle . \quad (2)$$

It is clear that only the linear combinations of the helicity amplitudes that are invariant under P and T can contribute to Compton scattering. It is easy to see that there are $2(J+1)(2J+1)$ independent helicity amplitudes for a spin-J target. Thus there are two independent amplitudes for a spin-0 target, six for a spin-1/2 target, and twelve for a spin-1 target, such as deuteron. The twelve amplitude structures for deuteron Compton scattering can be further classified as the scalar, vector and tensor amplitudes, S , V and T :

$$A = \frac{ie^2}{2M_N} \left[S \epsilon'_d \cdot \epsilon_d + \epsilon_{ijk} V_i \epsilon'_{d_j} \epsilon_{d_k} + T_{ij} \left(\epsilon'_{d_i} \epsilon_{d_j} + \epsilon_{d_i} \epsilon'_{d_j} - \frac{2}{3} \delta_{ij} \epsilon'_d \cdot \epsilon_d \right) \right] , \quad (3)$$

where ϵ_d (ϵ'_d) is the initial(final) deuteron polarization, e is the proton charge and M_N is the nucleon mass. By the same counting discussed above, S , V and T have two, four and six independent structures, respectively. We chose the following basis for these amplitudes [31]:

$$S = f_1 \epsilon'^* \cdot \epsilon + f_2 \mathbf{s}'^* \cdot \mathbf{s} , \quad (4)$$

$$V_i = f_3 (\epsilon'^* \times \epsilon)_i + f_4 (\mathbf{s}'^* \times \mathbf{s})_i + f_5 \left(\mathbf{s}'^* \cdot \epsilon \hat{\mathbf{k}}_i - \epsilon'^* \cdot \mathbf{s} \hat{\mathbf{k}}'_i \right) + f_6 \left(\mathbf{s}'^* \cdot \epsilon \hat{\mathbf{k}}'_i - \epsilon'^* \cdot \mathbf{s} \hat{\mathbf{k}}_i \right) , \quad (5)$$

$$\begin{aligned} T_{ij} = & f_7 \epsilon'^*_i \epsilon_j + f_8 \mathbf{s}'^*_i \mathbf{s}_j + f_9 \left(\epsilon'^* \cdot \hat{\mathbf{k}} \hat{\mathbf{k}}'_i \epsilon_j + \epsilon \cdot \hat{\mathbf{k}}' \hat{\mathbf{k}}_i \epsilon'^*_j \right) + f_{10} \left(\mathbf{s}'^* \cdot \hat{\mathbf{k}} \hat{\mathbf{k}}'_i \mathbf{s}_j + \mathbf{s} \cdot \hat{\mathbf{k}}' \hat{\mathbf{k}}_i \mathbf{s}'^*_j \right) \\ & + f_{11} \frac{1}{2} \left(\hat{\mathbf{k}}_i \hat{\mathbf{k}}_j + \hat{\mathbf{k}}'_i \hat{\mathbf{k}}'_j \right) \epsilon'^* \cdot \epsilon + f_{12} \frac{1}{2} \left(\hat{\mathbf{k}}_i \hat{\mathbf{k}}_j + \hat{\mathbf{k}}'_i \hat{\mathbf{k}}'_j \right) \mathbf{s}'^* \cdot \mathbf{s} - \text{trace} , \end{aligned} \quad (6)$$

where $\epsilon(\epsilon')$ is the polarization for the initial(final) photon and $\hat{\mathbf{k}}(\hat{\mathbf{k}}')$ is the unit vector in the direction of the initial(final) photon momentum, $\mathbf{s} = \hat{\mathbf{k}} \times \epsilon$ and $\mathbf{s}' = \hat{\mathbf{k}}' \times \epsilon'$.

For unpolarized Compton scattering, the amplitude squared is proportional to

$$|A|^2 \propto |S|^2 + \frac{2}{3} |V_i|^2 + \frac{4}{3} |T_{ij}|^2 , \quad (7)$$

after summing over the initial and final deuteron polarizations. As we shall see in the following section, the $|S|^2$ term starts to contribute at $\mathcal{O}(Q^0)$ while α_0 and β_0 contribute at $\mathcal{O}(Q^2)$. The $|V_i|^2$ term also contributes at $\mathcal{O}(Q^2)$ while the $|T_{ij}|^2$ term only contributes at $\mathcal{O}(Q^3)$. The $|V_i|^2$ term should be included in a $\mathcal{O}(Q^2)$ calculation to extract α_0 and β_0

III. UNPOLARIZED CROSS SECTION FROM EFT

In the dibaryon formulation of the pion-less effective field theory [21, 24, 28], the nucleon field N and the 3S_1 -channel di-baryon field t_j are introduced. The effective lagrangian is

$$\mathcal{L} = N^\dagger \left(iD_0 + \frac{\mathbf{D}^2}{2M_N} \right) N - t_j^\dagger \left[iD_0 + \frac{\mathbf{D}^2}{4M_N} - \Delta \right] t_j - y \left[t_j^\dagger N^T P_j N + \text{h.c.} \right] \quad (8)$$

where $P_i = \tau_2 \sigma_2 \sigma_i / \sqrt{8}$ is the 3S_1 two-nucleon projection operators and y is a coupling constant between the dibaryon and two-nucleon in the same channel. The covariant derivative is $\mathbf{D} = \vec{\partial} + ieQ\mathbf{A}$ with $Q = (1 + \tau^3)/2$ as the charge operator and \mathbf{A} the photon vector potential. The nucleon-nucleon scattering amplitude is reproduced by the following choice of parameters

$$y^2 = \frac{8\pi}{M_N^2 r^{({}^3S_1)}}; \quad \Delta = \frac{2}{M_N r^{({}^3S_1)}} \left(\frac{1}{a^{({}^3S_1)}} - \mu \right) \quad (9)$$

where $a^{({}^3S_1)}$ is the scattering length, $r^{({}^3S_1)}$ is the effective range, and μ is the renormalization scale in the power divergent subtraction scheme [18] which conserves gauge symmetry. Similarly, one can introduce the dibaryon field S_i in the 1S_0 channel.

The magnetic coupling in the lagrangian is

$$\mathcal{L}_B = \frac{e}{2M_N} N^\dagger (\mu_0 + \mu_1 \tau_3) \sigma \cdot \mathbf{B} N + \left[e \frac{L_1}{M_N \sqrt{r^{({}^1S_0)} r^{({}^3S_1)}}} t_j^\dagger S_3 B_j + \text{h.c.} \right] - i \frac{e}{M_N} \left(\mu_0 - \frac{L_2}{r^{({}^3S_1)}} \right) \varepsilon^{ijk} t_i^\dagger B_j t_k, \quad (10)$$

where $\mu_0 = (\mu_p + \mu_n)/2$ and $\mu_1 = (\mu_p - \mu_n)/2$ are the isoscalar and isovector nucleon magnetic moments in units of nuclear magneton, and \mathbf{B} is the external magnetic field. L_1 has been determined by the rate of $np \rightarrow d\gamma$ [28, 30]. The measured cross section $\sigma^{\text{exp}} = 334.2 \pm 0.5$ mb with incident neutron speed of 2200 m/s fixes $L_1 = -4.42$ fm. L_2 is determined by the magnetic moment of the deuteron

$$\mu_d = 2\mu_0 + \frac{2\gamma L_2}{1 - \gamma r^{({}^3S_1)}} , \quad (11)$$

in units of nuclear magneton, where $\gamma = \sqrt{M_N B} = 45.703$ MeV with the deuteron binding energy $B = 2.225$ MeV. Fitting to the experimental value, one finds, $L_2 = -0.03$ fm.

The relativistic correction of the above nucleon magnetic interaction is the “spin-orbit” interaction

$$\mathcal{L}_{SO} = N^\dagger i \left[\left(2\mu_0 - \frac{1}{2} \right) + \left(2\mu_1 - \frac{1}{2} \right) \tau_3 \right] \frac{e}{8M_N^2} \sigma \cdot (\mathbf{D} \times \mathbf{E} - \mathbf{E} \times \mathbf{D}) \mathbf{N} , \quad (12)$$

where \mathbf{E} is an external electric field. There are also polarizability contributions

$$\begin{aligned} \mathcal{L}_{pol} = & 2\pi N^\dagger (\alpha_0 + \alpha_1 \tau_3) \mathbf{E}^2 N + 2\pi N^\dagger (\beta_0 + \beta_1 \tau_3) \mathbf{B}^2 N \\ & + \frac{2\pi \alpha_4}{M_N r^{({}^3S_1)}} t_i^\dagger t_i \mathbf{E}^2 + \frac{2\pi \beta_4}{M_N r^{({}^3S_1)}} t_i^\dagger t_i \mathbf{B}^2 \end{aligned} \quad (13)$$

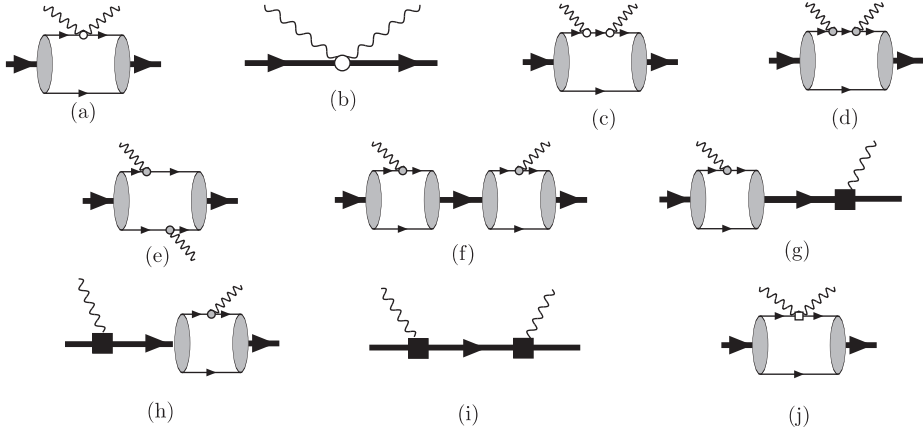


FIG. 1: Feynman diagrams for the scalar amplitude of deuteron Compton scattering. The thick initial and final state arrows represent the deuteron. The thick arrows in the middle of the diagrams are the dibaryon states in the 3S_1 and 1S_0 channels. The open circles denote the electric current interactions, and the shaded circles the magnetic moment interactions. The solid squares are from electromagnetic counter-terms (L_1 and L_2). The open square is from the nucleon polarizabilities.

where $\alpha_{0,1} = (\alpha_p \pm \alpha_n)/2$ is the isoscalar (isovector) nucleon electric polarizability, and $\beta_{0,1} = (\beta_p \pm \beta_n)/2$ is the isoscalar (isovector) magnetic polarizability. α_4 and β_4 are unknown two-body currents which will limit the precision of extractions of the above polarizabilities in deuteron Compton scattering.

In this version of EFT with pions integrated out, the ultraviolet cut-off scale Λ is typically set by the pion mass $m_\pi \simeq 140$ MeV, although the nucleon mass comes in from the nucleon propagator. Following [28], we will not distinguish the difference between M_N and m_π . There are some light scales denoted as Q in the system. The inverse scattering lengths $1/a^{(i)}$ and deuteron internal momentum γ are of order Q while the effective ranges $r^{(i)}$ are counted as $1/Q$. This counting allows the re-summation of the effective range contributions, which is a distinctive feature of the dibaryon approach. Note that in another approach, $r^{(i)}$ is counted as Q^0 [18, 25], thus the effective range contributions are perturbative.

The photon energy ω scales as Q^2 at energies comparable and below the deuteron binding (region I) and as Q at higher energies (region II) [27]. Since the nucleon polarizability contributions are proportional to ω^2 , we will work in region II to accentuate their effects. Another scale in the problem is the relative momentum p between the nucleons in the intermediate states. Naively, $p \sim \sqrt{M_N \omega}$, thus one expects $p \sim \Lambda$ when $\omega \sim 30$ MeV. However, for the unpolarized deuteron Compton scattering, the pionless theory still converges well at $\omega \sim 50$ MeV. This is because the main uncertainty from diagrams with nucleon-nucleon rescattering in intermediate states are generally suppressed compared to the non-rescattering ones. Furthermore, the uncertainty is mainly from the P waves and higher, because the S-wave rescattering is described by the pionless EFT well in this energy range.

Despite the successes of the pionless EFT, it is important that future experiments can be measured at lower energies such that the theory is unquestionably under control. We will explore the optimal energy range in the end of this section.

Diagrams contributing to the scalar amplitude S (or equivalently f_1 and f_2) to $\mathcal{O}(Q^2)$ are shown in Fig.1. The gauge-coupling diagrams in 1(a) and 1(b) are of order Q^0 , and of order $Q^{1/2}$ in 1(c). The magnetic diagrams in 1(d) is of order Q and of order $Q^{3/2}$ in 1(e),

while those in 1(f)-1(i) are of order Q^2 , with the solid squares denoting magnetic two-body current L_1 and L_2 . The open square in 1(j) is the nucleon polarizability coupling which also contributes at Q^2 .

The results of the diagrams are expressed in terms of the reduced amplitudes

$$f_i = \frac{1}{(1 - \gamma r^{(3S_1)})} \tilde{f}_i , \quad (14)$$

where $i = 1 - 12$. We write

$$\begin{aligned} \tilde{f}_1 &= g_1(\omega) + g_1(-\omega) + zh(\omega) , \\ \tilde{f}_2 &= g_2(\omega) + g_2(-\omega) - h(\omega) , \end{aligned} \quad (15)$$

where

$$\begin{aligned} g_1(\omega) &= \left[\frac{\gamma \rho_d}{2} - \frac{4\gamma}{\sqrt{2-2z}\omega} \tan^{-1}\left(\frac{\sqrt{2-2z}\omega}{4\gamma}\right) + \frac{2\gamma \left(\gamma + 2\sqrt{\gamma^2 - \omega M_N - i\varepsilon}\right)}{3\left(\gamma + \sqrt{\gamma^2 - \omega M_N - i\varepsilon}\right)^2} \right. \\ &\quad \left. + \frac{32\pi\gamma\omega M_N \alpha_0}{e^2\sqrt{2-2z}} \tan^{-1}\left(\frac{\sqrt{2-2z}\omega}{4\gamma}\right) \right] , \end{aligned} \quad (16)$$

and

$$\begin{aligned} h(\omega) &= \frac{1}{15\omega^2 M_N^4} \left(-4\gamma(\gamma^2 - \omega M_N - i\varepsilon)^{\frac{5}{2}} + 8\gamma^6 + 20\gamma^4\omega M_N + 60\gamma^2\omega^2 M_N^2 \right. \\ &\quad \left. + 15\omega^3 M_N^3 - \gamma\sqrt{\gamma^2 + \omega M_N} (4\gamma^4 + 28\gamma^2\omega M_N + 39\omega^2 M_N^2) \right) . \end{aligned} \quad (17)$$

and where

$$g_2(\omega) = \frac{32\pi\gamma\omega M_N \beta_0}{e^2\sqrt{2-2z}} \tan^{-1}\left(\frac{\sqrt{2-2z}\omega}{4\gamma}\right) + \frac{4\gamma \left(\gamma - \sqrt{\gamma^2 - \omega M_N - i\varepsilon}\right) \mu_1^2}{3M_N^2} + k(\omega) , \quad (18)$$

and

$$k(\omega) = -\frac{\gamma \left[\omega L_1 M_N + 2 \left(\gamma - \sqrt{\gamma^2 - \omega M_N - i\varepsilon} \right) \mu_1 \right]^2}{3M_N^2 \left(\frac{1}{a^{(1S_0)}} - \sqrt{\gamma^2 - \omega M_N - i\varepsilon} + \frac{r^{(1S_0)}}{2} (\gamma^2 - \omega M_N) \right)} . \quad (19)$$

These results agree with those obtained in the previous calculations [28, 29]. If the effective range is counted as order Q^0 instead of Q^{-1} then the results of Ref. [29] are reproduced. Also, the results of Ref. [28] are reproduced up to recoil effects which can be safely neglected.

The new contributions we calculate are shown in Fig. 2. Those are diagrams contributing to the vector amplitude V or, equivalently, the amplitudes $f_{3,\dots,6}$. The solid circle denotes the spin-orbit coupling in Eq. (12). The leading diagrams are 2(a)-2(c) which are of order Q . It is interesting to note that the relativistic correction (the spin-orbit interaction in diagram 2(a)) contributes at leading order. Diagram 2(d) is of order $Q^{3/2}$, while diagrams 2(e)-2(h) are of order Q^2 . Naively, if we want to calculate the cross section to order Q^2 , these orders $Q^{3/2}$ and Q^2 diagrams are not needed according to Eq. (7). We still choose

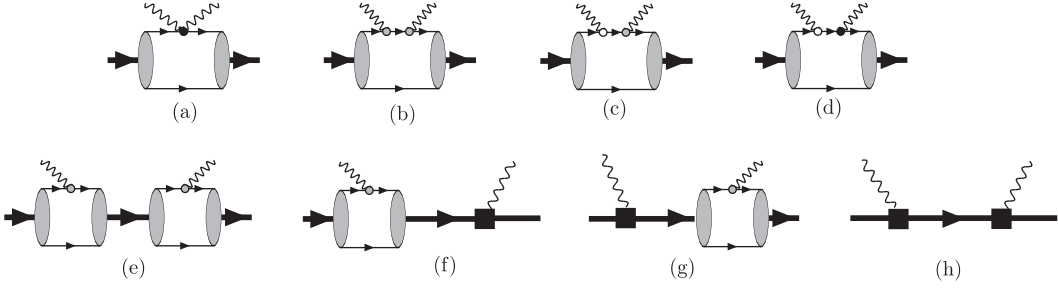


FIG. 2: Feynman diagrams for the vector amplitude of deuteron Compton scattering. The solid circles denote the spin-orbit intercation in Eq. (12). Other symbols are the same as described in Fig. 1.

to include these contributions because there is an enhancement factor $\mu_1^2 \sim 5.5 \sim 1/Q$ in them. The diagrams give

$$\begin{aligned}\tilde{f}_3 &= g_3(\omega) - g_3(-\omega) + 2q(\omega) , \\ \tilde{f}_4 &= g_4(\omega) - g_4(-\omega) , \\ \tilde{f}_5 &= 0 , \\ \tilde{f}_6 &= -q(\omega) ,\end{aligned}\quad (20)$$

where

$$g_3 = \frac{2\gamma(2\mu_0 + 2\mu_1 - 1)}{M_N} \left[\frac{1}{\sqrt{2-2z}} \tan^{-1}\left(\frac{\sqrt{2-2z}\omega}{4\gamma}\right) \right] . \quad (21)$$

$$\begin{aligned}q(\omega) &= -\frac{(\mu_0 + \mu_1)}{3\omega M_N^3 \sqrt{\gamma^2 + \omega M_N}} \left[-2\gamma^5 + 2\gamma^3 \sqrt{\gamma^2 + \omega M_N - i\varepsilon} \left(2\gamma - \sqrt{\gamma^2 - \omega M_N - i\varepsilon} \right) \right. \\ &\quad + \gamma\omega M_N \left(-7\gamma^2 + 3\gamma\sqrt{\gamma^2 + \omega M_N} + 2\sqrt{\gamma^4 - \omega^2 M_N^2 - i\varepsilon} \right) \\ &\quad \left. + \omega^2 M_N^2 \left(-5\gamma + 3\sqrt{\gamma^2 + \omega M_N} \right) \right] ,\end{aligned}\quad (22)$$

and

$$g_4(\omega) = \frac{3}{2}k(\omega) - (\mu_0^2 + \mu_1^2) \left[\frac{\omega}{M_N} + \frac{2\gamma}{M_N^2} \sqrt{\gamma^2 - \omega M_N - i\varepsilon} \right] , \quad (23)$$

with $k(\omega)$ as given in Eq. (19).

As noted above, the tensor amplitude T only contributes to the cross section at (Q^3) . At the same order, unknown two-body currents α_4 and β_4 defined in Eq. (13) also contribute. Thus we just calculate the unpolarized Compton scattering to order Q^2 . This will allow us to extract the nucleon electric polarizability α_0 with $\sim 30\%$ theoretical uncertainty.

Combining the above results, the differential cross section for unpolarized Compton scattering is

$$\begin{aligned}\left. \frac{d\sigma}{d\Omega} \right|_{cm} &= \frac{\alpha^2}{6(\omega + 2M_N)^2} \text{Re} \left[3(1 + z^2)(f_1^* f_1 + f_2^* f_2) + 12z f_1^* f_2 \right. \\ &\quad + 2(3 - z^2)(f_3^* f_3 + f_4^* f_4) + 8z f_3^* f_4 + 4(1 + 3z^2)(f_5^* f_5 + f_6^* f_6) \\ &\quad \left. + 8z(3 + z^2)f_5^* f_6 + 8(1 + z^2)(f_3^* f_6 + f_4^* f_5) + 16z(f_3^* f_5 + f_4^* f_6) \right] ,\end{aligned}\quad (24)$$

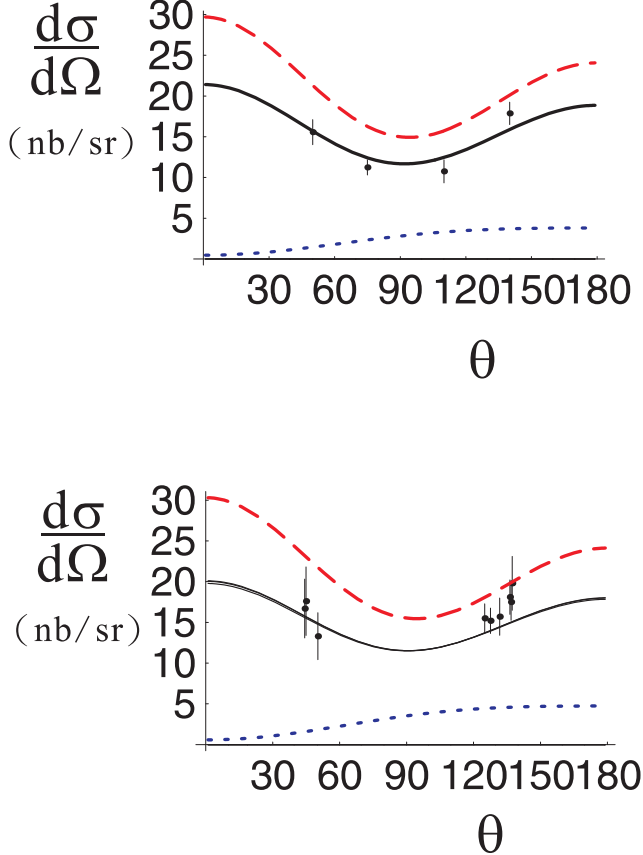


FIG. 3: Differential cross section for $\gamma d \rightarrow \gamma d$ with incident photon energy $\omega = 49$ MeV (upper plot) and $\omega = 55$ MeV (lower plot). The dashed curves are $\mathcal{O}(Q^2)$ results with no nucleon polarizabilities, $\alpha_0 = \beta_0 = 0$. The solid curves are results using polarizabilities $\alpha_0 = 10\beta_0 = 1.2 \times 10^{-3}$ fm³, calculated in leading order chiral perturbation theory [20]. The dotted curves are the vector amplitudes contributions alone. The 49 MeV data is from Ref. [10], while the 55 MeV data is from Ref. [12].

where $\alpha = 1/137$ is the fine structure coupling constant and $z = \cos \theta = \hat{\mathbf{k}} \cdot \hat{\mathbf{k}}'$.

In Fig. 3, we show the differential cross section for $\omega = 49$ MeV (upper plot) and $\omega = 55$ MeV (lower plot). The 49 MeV data is measured at Illinois while the 55 MeV data is actually a superposition of the 54.6, 54.9 and 55.9 MeV data from the Lund experiment. In both plots, the dashed curves are $\mathcal{O}(Q^2)$ results with no nucleon polarizabilities, $\alpha_0 = \beta_0 = 0$. The solid curves are results using nucleon polarizabilities calculated in leading order chiral perturbation theory (ChPT) [20],

$$\alpha_0 = 10\beta_0 = \frac{5g_A^2 e^2}{192\pi^2 f_\pi^2 m_\pi} = 1.2 \times 10^{-3} \text{ fm}^3. \quad (25)$$

The dotted curves are the contributions of the vector amplitudes which were not included in the previous calculations [27, 28, 29]. These effects are $\sim 20\%$ and are as large as the nucleon polarizability contributions in the backward angles.

In Fig. 4 we plot the cross section using the counting employed in Ref. [29] and the value of Eq. (25). We set $1/a^{(i)} \sim \omega \sim Q$, $r^{(i)} \sim Q^0$ (such that the effective range contributions

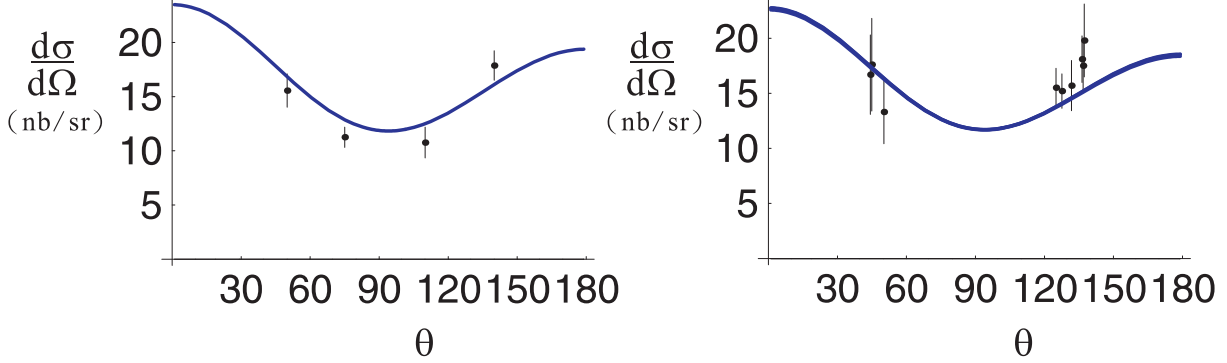


FIG. 4: Differential cross section for $\gamma d \rightarrow \gamma d$ with incident photon energy $\omega = 49$ MeV (left plot) and $\omega = 55$ MeV (right plot). The leading-order ChPT values $\alpha_0 = 10\beta_0 = 1.2 \times 10^{-3}$ fm 3 are used and the effective range parameter is treated as order Q^0 .

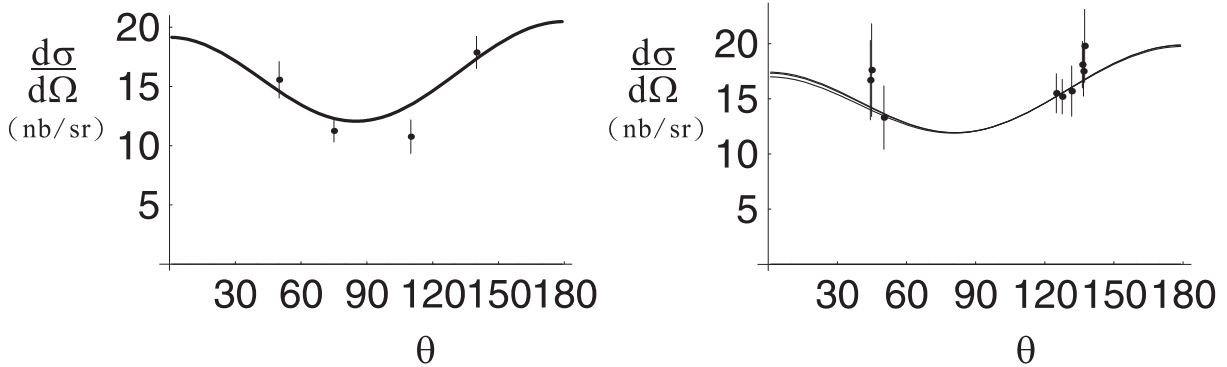


FIG. 5: Differential cross section for $\gamma d \rightarrow \gamma d$ with incident photon energy $\omega = 49$ MeV (left plot) and $\omega = 55$ MeV (right plot). The best fit value $\alpha_0 = 12.3$ and $\beta_0 = 5.0$ (in units of fm $^{-4}$) are used and all data points are assumed to be independent in the fitting.

are treated perturbatively) and expand our amplitudes in Q . The leading order ChPT value of nucleon polarizabilities also gives a good description of data. Setting the vector amplitude to be zero, our result coincides with that of Fig. 2 of Ref. [29].

Assuming the data measured at $\omega = 49, 54.6, 54.9$ and 55.9 MeV are independent, a χ^2 fit gives $\alpha_0 = 12.3 \pm 1.4$ and $\beta_0 = 5.0 \pm 1.6$ (note that theoretical uncertainty is not included) in the dibaryon formalism. The best fit curves are plotted in Fig. 5. In the counting that treats the effective range perturbatively, the χ^2 fit gives $\alpha_0 = 14.2 \pm 2.1$ and $\beta_0 = 9.3 \pm 2.5$ (theoretical uncertainty is not included) with very similar curves as those shown in Fig. 5. The difference between these two counting schemes is of higher order, thus it appears that while the fit values of α_0 are quite close to the one predicted by leading order ChPT, the error on β_0 is quite large using the current data. These results can be compared with $\alpha_0 = 8.4 \pm 3.4$ and $\beta_0 = 8.9 \pm 4.3$ from Ref. [29], where the contribution of the vector amplitude has been neglected. Thus the vector amplitude has significant effect on a reliable extraction of α_0 .

Future high energy, high precision experiments can take advantage of the theoretically clean pionless EFT by performing the measurement at lower energies. However, the nucleon polarizability contributions become less important at lower energies. To study the best en-

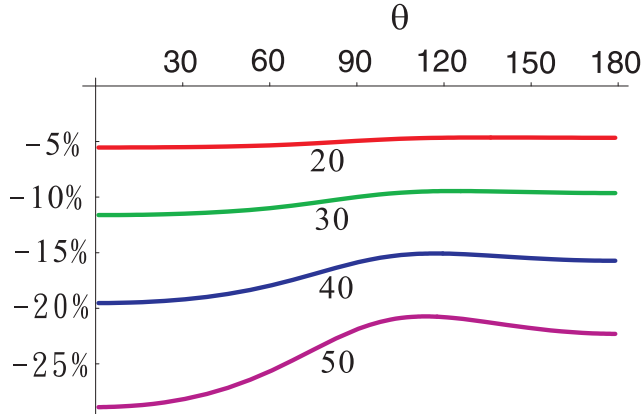


FIG. 6: Nucleon polarizability effects on Compton scattering cross section with $\alpha_0 = 10\beta_0 = 12$ (in units of 10^{-4} fm 3). The curves, from top to bottom, are for photon energy $\omega = 20, 30, 40$ and 50 MeV, respectively.

ergy range for future experiments, we show the nucleon polarizability effects in the Compton scattering cross section for $\alpha_0 = 10\beta_0 = 12$ (the leading order ChPT value) in Fig. 6. The curves, from top to bottom, are for photon energy $\omega = 20, 30, 40$ and 50 MeV, respectively. Given the unknown $\mathcal{O}(Q^{5/2})$ effect is about 5% for a series with expansion parameter $\sim 1/3$ and the theory converges better at $\lesssim 30$ MeV, we recommend the best energy range to perform the deuteron Compton measurement is 25-35 MeV. From this figure, we see that a measurement at 30 MeV with 3% error will constrain α_0 with 3×10^{-4} fm 3 experimental error, which is comparable to the expected theoretical error.

IV. CONCLUSION

We have computed the unpolarized Compton scattering in dibaryon effective field theory at $\mathcal{O}(Q^2)$. The vector amplitude, which contributes to the cross section at $\mathcal{O}(Q^2)$ but was not included in previous pionless EFT calculations, was found to affect the extraction of nucleon electric polarizability by more than 50% at 49 MeV. We recommend future high precision deuteron Compton scattering experiments be measured at 25-35 MeV photon energy for appreciable nucleon polarizability effects and controllable theoretical higher-order effects. More specifically, a measurement at 30 MeV with 3% error will constrain α_0 with 3×10^{-4} fm 3 experimental error, which is comparable to the expected theoretical error.

This work was supported by the U. S. Department of Energy via grant DE-FG02-93ER-40762 and by the National Science Council of Taiwan, ROC. JWC thanks Paulo Bedaque for organizing the Summer of Lattice Workshop 2004 at Lawrence Berkeley Laboratory where part of this research was completed.

[1] P.S. Baranov *et al.*, Sov. J. Nucl. Phys. **21**, 355 (1975); A. Ziegler *et al.*, Phys. Lett. B **278**, 34 (1992); F.J. Federspiel *et al.*, Phys. Rev. Lett. **67**, 1511 (1991); E.L. Hallin *et al.*, Phys. Rev. C **48**, 1497 (1993); B.E. MacGibbon *et al.*, Phys. Rev. C **52**, 2097 (1995).
[2] V. Olmos de León *et al.*, Eur. Phys. J. A **10**, 207 (2001).

- [3] S.R. Beane, M. Malheiro, J.A. McGovern, D.R. Phillips, U. van Kolck, nucl-th/0403088; Phys. Lett. **B567**, 200 (2003); Nucl. Phys. **A656**, 367 (1999).
- [4] Yu.A. Aleksandrov, Phys. Part. Nucl. **32**, 708 (2001).
- [5] J. Schmiedmayer *et al.*, Phys. Rev. Lett. **66**, 1015 (1991).
- [6] L. Koester *et al.*, Phys. Rev. C **51**, 3363 (1995).
- [7] T.L. Enik *et al.*, Sov. J. Nucl. Phys. **60**, 567 (1997).
- [8] K. Kossert *et al.*, Phys. Rev. Lett. **88**, 162301 (2002).
- [9] M.I. Levchuk, A.I. L'vov, and V.A. Petrun'kin, FIAN report No. 86, 1986; Few-Body Syst. **16**, 101 (1994).
- [10] M.A. Lucas, Ph.D. thesis, University of Illinois, 1994.
- [11] D.L. Hornidge *et al.*, Phys. Rev. Lett. **84**, 2334 (2000).
- [12] M. Lundin *et al.*, Phys. Rev. Lett. **90**, 192501 (2003).
- [13] M. Weyrauch, Phys. Rev. **C41**, 880 (1990).
- [14] T. Wilbois, P. Wilhelm, and H. Arenhovel, Few-Body Systems Suppl. **9**, 263 (1995).
- [15] J. J. Karakowski and G. A. Miller, Phys. Rev. **C60**, 014001(1999).
- [16] M.I. Levchuk and A.I. L'vov, Nucl. Phys. **A674**, 449 (2000); M.I. Levchuk and A.I. L'vov, Nucl. Phys. **A684**, 490 (2001).
- [17] S. Weinberg, Phys. Lett. **B251**, 288(1990); Nucl. Phys. **B363** 3(1991).
- [18] D. B. Kaplan, M. J. Savage and M.B. Wise, Phys. Lett. **B424**, 390(1998); D. B. Kaplan, M. J. Savage and M.B. Wise, Nucl. Phys. **B534**, 329(1998).
- [19] S. R. Beane, P. F. Bedaque, W. C. Haxton, D. R. Phillips, and M. J. Savage, nucl-th/0008064.
- [20] V. Bernard, N. Kaiser and Ulf-G. Meißner, *Phys. Rev. Lett.* **67**, 1515 (1991); *Nucl. Phys. B* **373**, 364 (1992); *Phys. Lett. B* **319**, 269 (1993).
- [21] D. B. Kaplan, Nucl. Phys. **B494**, 471(1997).
- [22] U. van Kolck, hep-ph/9711222; Nucl. Phys. **A645** 273 (1999).
- [23] T.D. Cohen, Phys. Rev. **C55**, 67 (1997); D.R. Phillips and T.D. Cohen, Phys. Lett. **B390**, 7 (1997); S.R. Beane, T.D. Cohen, and D.R. Phillips, Nucl. Phys. **A632**, 445 (1998).
- [24] P.F. Bedaque and U. van Kolck, Phys. Lett. **B428**, 221 (1998).
- [25] J. W. Chen, G. Rupak, and M. J. Savage, Nucl. Phys. **A653**, 386 (1999).
- [26] S.R. Beane, P.F. Bedaque, M.J. Savage, and U. van Kolck, Nucl. Phys. **A700**, 377 (2002).
- [27] J.W. Chen, H.W. Grießhammer, M.J. Savage, R.P. Springer, Nucl. Phys. **A644**, 245(1998); J.W. Chen, Nucl. Phys. **A653**, 375(1999).
- [28] S. R. Beane and M. J. Savage, Nucl. Phys. **A694**, 511 (2001).
- [29] H. W. Grießhammer and G. Rupak, Phys. Lett. **B529**, 57 (2002).
- [30] J.W. Chen and M.J. Savage, Phys. Rev. **C60**, 065205 (1999).
- [31] J.W. Chen, Y. Li and X. Ji, in preparation.